Polym. Bull. (2016) 73:3183–3208
DOI 10.1007/s00289-016-1649-8

ORIGINAL PAPER

Synthesis and characterization of pH-sensitive superabsorbent hydrogels based on sodium alginate-*g*-poly(acrylic acid-*co*-acrylamide) obtained via an anionic surfactant micelle templating under microwave irradiation

Mohammad Tally[1] · Yomen Atassi[1]

Received: 4 October 2015 / Revised: 8 February 2016 / Accepted: 16 March 2016 /
Published online: 23 March 2016
© Springer-Verlag Berlin Heidelberg 2016

Abstract A novel porous superabsorbent polymer based on poly(acrylic acid-co-acrylamide) grafted onto sodium alginate backbone was prepared under microwave irradiation. Anionic surfactant sodium *n*-dodecyl benzenesulfonate (SDBS) is used as a pore-forming micelle templating. FTIR spectroscopy confirmed the formation of the gel and removal of SDBS by washing. The swelling behaviors in distilled water and in solutions with different pH values are investigated. The results indicate that there is an optimized concentration of SDBS (1.92 mM) where the swelling rate (63.84 g g^{-1} min^{-1}) and the swelling capacity (1078 g/g) are maximal. These results are also supported by scanning electron microscopy where the optimized hydrogel exhibits higher pore sizes and interconnected open cellular structure. The optimized hydrogel is used as adsorbent for metal ion Pb(II). Isotherm of adsorption and effect of pH, adsorption dosage and recyclability are discussed. The results show that maximum adsorption capacity of Pb(II) on the hydrogel is 480.77 $mg.g^{-1}$ and adsorption is well described by Langmuir isotherm model. Adsorption capacity of the optimized hydrogel for other hazardous heavy metal ions Cd(II), Ni(II) and Cu(II) and their competitive adsorption are also investigated.

Keywords Hydrogel · SDBS micelle templating · Polyacrylate · Polyacrylamide · Heavy metal removal

✉ Yomen Atassi
yomen.atassi@gmail.com; yomen.atassi@hiast.edu.sy

[1] Laboratory of Materials Science, Department of Applied Physics, Higher Institute for Applied Science and Technology, P.O. Box 31983, Damascus, Syria

Introduction

Superabsorbent polymers (SAPs) are water-swellable, three-dimensional, slightly crosslinked hydrophilic polymeric network [1]. These materials can absorb large amounts of water and even retain the absorbed water under some pressure [2].

In the development and design of new SAPs some considerations and features are of especial importance as: high swelling capacity, fast swelling rate, biodegradability, low production cost and good gel strength. Among these properties, swelling rate is important because it determines the application properties of SAPs in almost each field [3]. Recently, many efforts have been made to improve the swelling rate of the superabsorbents for improving their applicability [4].

In principle, the initial swelling rate of a superabsorbent is primarily due to the penetration of water molecules into the polymeric network through diffusion and capillarity [5]. Higher porosity in the superabsorbents can increase the contact area between polymeric network and external solution that facilitates to speed up the diffusion rate [6]. So, the creation of porosity structure in the hydrogels is the key to enhance the swelling rate of superabsorbents and to regulate the properties [3, 7].

Currently, there are various available techniques for fabricating porous hydrogels mainly include freeze-drying and hydration technique [8], foaming technique [9], water-soluble porogens [10] and phase inversion technique [11]. However, these techniques often yield hydrogels with broad macropore size distributions with a mixture of open and closed pores [12, 13].

Surfactants can self-assemble to form micelles in aqueous environment, which act as a template in the polymerization reaction process to form porous materials with well-defined and controlled pore size. They were applied in drug delivery systems [14], tissue engineering [15] and wastewater treatment [16].

Contamination of water resources by organic pollutants and heavy metals has become an issue of great concern due to the harmful effects on living beings and even on the whole ecological system. Several kinds of techniques have been attempted to remove these pollutants, such as photocatalysis for the decomposition of organic pollutants [17–19], electrosorption for removal of heavy ions [20], adsorption onto amino-functionalized ordered mesoporous silica [21], etc. Recently, the use of hydrogel polymers for removal of heavy metal ions and dyes from wastewater has become subject of great interest owing to their high absorption capacity, selectivity and reusability. The presence of functional groups within polymeric network helps in binding the pollutants via formation of complex structures [22–24].

The porosity of hydrogels can affect water uptake of hydrogels and their ability for pollutant adsorption. Using micelle templating is an effective way that can be used to increase porosity of hydrogels [12].

On the other hand, hydrogels based on bio-resources are promising candidates as bio-adsorbents since they are less expensive than conventional adsorbents, such as ion-exchange resins or activated carbon.

Sodium alginate (NaAlg) is an anionic polysaccharide, which is composed of poly- β-1, 4-D-mannuronic acid (M units) and α-1, 4-L-glucuronic acid (G units) in

varying proportions by 1–4 linkages. NaAlg can be extracted from brown algae. It is abundant, renewable, non-toxic, water soluble, biodegradable and biocompatible [25].

Conventional thermal heating methods usually take a long time and consume much energy. However, microwave heating is a promising heating technique due to its specificity in terms of reactivity and its rapid bulk heating capability [26–29]. Currently, the graft copolymerization of vinyl monomers onto natural polymers has been successfully conducted under microwave irradiation [28].

In this study, we use microwave irradiation to prepare sodium alginate (NaAlg) graft copolymerized with partially neutralized acrylic acid (AA) and acrylamide (AM): NaAlg-*g*-P(AA-*co*-AM). The porosity of the novel sodium alginate superabsorbent polymers is due to micelle templating formed by the self-assembled anionic surfactant sodium *n*-dodecyl benzene sulfonate (SDBS). Fourier transform infrared (FTIR) spectroscopy is used to confirm the successful synthesis of NaAlg-*g*-P(AA-*co*-AM) hydrogel and removal of SDBS from the products by washing process. X-ray patterns are also used to verify the grafting reaction. The effect of SDBS concentration on the porosity of the prepared superabsorbents is investigated by scanning electron microscopy (SEM). In addition, the swelling kinetics of these SAPs as function of SDBS concentration and pH of the medium are also studied. The ability of the prepared hydrogel in adsorption of metal ion Pb(II) is investigated. Isotherm of adsorption and effect of pH, adsorption dosage and recyclability are discussed. Adsorption capacity of the optimized hydrogel for other hazardous heavy metal ions Cd(II), Ni(II) and Cu(II) and their competitive adsorption are also investigated.

Experimental

Chemicals and materials

Sodium alginate (NaAlg, viscosity of the aqueous solution at a concentration of 1 % is 5.0–40.0 cps at 25 °C) and sodium dodecyl benzene sulfonate (SDBS, MW = 348.48 g/mol,) were purchased from Sigma-Aldrich. Acrylic acid (AA), for synthesis, and Acrylamide (AM), for synthesis, were from Merck and they were used as purchased. Potassium peroxodisulfate (KPS), GR for analysis, as an initiator, *N*,*N*′-methylene bisacrylamide (MBA), special grade for molecular biology, as a crosslinker, and *N*,*N*,*N*′,*N*′-tetramethylene diamine (TEMED) GR for analysis as an accelerator were also obtained from Merck. Sodium hydroxide NaOH microgranular pure (POCH) was used for acid neutralization. Solvents: methanol and ethanol (GR for analysis) were obtained from Merck. Saline sodium chloride (NaCl) (Merck), magnesium chloride ($MgCl_2$) (Merck) and aluminum chloride ($AlCl_3$) (Merck) were prepared with distilled water and were all purchased from Merck (GR for analysis). All the metal ion reagents (Pb(II), Ni(II), Cd(II) and Cu(II)) were nitrate salts and were of analytical grade. They were purchased from Merck and used without any purification.

Preparation of NaAlg-*g*-P(AA-*co*-AM) superabsorbent polymers SAPs

The general procedure for the preparation of the superabsorbent polymer through graft copolymerization of poly(AA-*co*-AM) onto NaAlg was conducted as follows:

The monomers solutions were prepared as follows: (6 g) AA was partially neutralized to 75 wt% by addition of NaOH solution (5 M) to the acid in an ice bath to avoid polymerization, then the solution is added to the solution of acrylamide (6 g in ca. 12 mL of distilled water) with continuous stirring. After that, we added the MBA solution (0.043 g in ca. 5 mL of distilled water).

NaAlg (1.20 g) was dissolved in 35 mL purified water under mechanical stirring at 60 °C for 15 min. Then aqueous solution of the surfactant SDBS with different concentrations (0, 0.96, 1.92, 2.88, and 3.84 mM) was added and the stirring of the mixture was continuing for 15 min to assure homogeneous solution formation. Two equimolar aqueous solutions of the redox initiator system of KPS, 0.118 g and TEMED, 0.051 g (each in ca. 5 mL of distilled water) were prepared and then dropwise added to the solution of NaAlg under vigorous mechanical stirring and kept at 60 °C for 10 min to generate radicals. After cooling this solution to 50 °C, the monomer solution was added dropwise on it, under continuous stirring at 1050 rpm for 15 min. The total volume of the reactive mixture is brought to 100 mL by adding distilled water. Then, the final mixture is treated in a microwave oven at the power of 475 W for 4 min. The mixture temperature and viscosity increase gradually and the gelation point is reached after 210 s.

The product (as an elastic yellow gel) is cut to small pieces. And it was firstly washed thoroughly with methanol/water (8:1, v/v) for several times to remove the surfactant and then was immersed 24 h in absolute methanol for dehydration and dissolving non-reacting reagent. At last, it was washed by ethanol, and dried for several hours at 60 °C until it became solid and brittle. At this point the solid was milled and treated in the furnace at 60 °C for 24 h.

Instrumental analysis

The IR spectra in the 400–4000 cm^{-1} range were recorded at room temperature on the infrared spectrophotometer (Bruker, Vector 22). For recording IR spectra, powders were mixed with KBr in the ratio 1:250 by weight to ensure uniform dispersion in the KBr pellet. The mixed powders were then pressed in a cylindrical die to obtain clean discs of approximately 1 mm thickness.

The morphology of the samples was examined using scanning electron microscope VEGA II TESCAN SEM instrument after coating the samples with graphite.

Thermogravimetric analyses of sodium alginate NaAlg, and the superabsorbent hydrogel were performed (SETARAM, Labsys TG, 1600 °C) from room temperature to 400 °C at a heating rate of 10 °C/min and under argon atmosphere.

A computer interface X-ray powder diffractometer (Philips, X'pert) with Cu Kα radiation ($\lambda = 0.1542$ nm) was used to identify the crystalline phases. The data collection was over the 2-theta range of 10–70° in steps of 0.02° s^{-1}.

Atomic absorption spectrophotometer (AAS) Shimadzu, AA-6800 was used to measure the adsorbance of heavy metals on the superabsorbent hydrogel.

Swelling measurements

Water absorbency of the hydrogel is measured by the free swelling method and is calculated in grams of water per 1 g of the hydrogel. Thus, an accurately weighed quantity of the polymer under investigation (0.1 g) is immersed in 500 mL of distilled water at room temperature for at least 4 h. Then the swollen sample is filtered through weighed 100-mesh (150 μm) sieve until water ceased to drop.

The weight of the hydrogel containing absorbed water is measured after draining and the water absorbency is calculated according to the following Eq. (1):

$$S_{\text{eq}} = (w_s - w_d)/w_d \tag{1}$$

where S_{eq} is the equilibrium water absorption calculated as grams of water per gram of superabsorbent sample; w_d and w_s are the weights of the dry sample and swollen sample, respectively [30, 31].

Gel content

To measure the gel content, accurately weighed dried samples of SAPs NaAlg-*g*-P(AA-*co*-AM) are dispersed in distilled water to swell completely. Then the swollen SAPs are filtered and washed with distilled water frequently. The samples are dewatered in excess ethanol for 48 h, and dried at 50 °C for 12 h until the SAPs have a constant weight. The gel content is defined as the following equation [32]:

$$\text{Gel } (\%) = \frac{W_d}{W_i} \times 100 \tag{2}$$

where W_d is the weight of dried SAPs after extraction and W_i is the initial weight of the SAPs.

Grafting percentage and grafting efficiency

The grafting percentage (G %) and the grafting efficiency (E %) were calculated according to the Eqs. (3), (4), [33–35]:

$$G\,\% = \frac{W_1 - W_0}{W_0} \times 100 \tag{3}$$

$$E\,\% = \frac{W_1 - W_0}{W_2} \times 100 \tag{4}$$

where W_0, W_1, W_2 denote the weight of NaAlg, final weight of the grafted hydrogel and weight of monomers, respectively.

Water retention

The pre-weighed swollen gels (w_3) equilibrated in distilled water are left at room temperature for 24 h. Then, the mass of hydrogels is recorded and marked as w_4. The percentage water retention is calculated as follows [36]:

$$\text{Water retention } (\%) = \frac{w_4}{w_3} \times 100 \tag{5}$$

Swelling kinetics at different SDBS concentrations

Accurately weighed quantities (0.1 g) of SAP prepared from different concentrations of SDBS (0, 0.96, 1.92, 2.88, and 3.84 mM) are immersed in 500 mL of distilled water at room temperature. At consecutive time intervals, the water absorbency of the SAP is measured according to Eq. (1).

Swelling kinetics at different pH values

To investigate the rate of absorbency of the SAP at different pH values, accurately weighed quantities (0.1 g) of the hydrogel NaAlg-*g*-P(AA-*co*-AM) prepared at a concentration of SDBS equals 1.92 mM are immersed in 500 mL of aqueous solutions of different pH values (pH 4.0, 7.0 and 12.0) at room temperature. At consecutive time intervals, the water absorbency of the SAP is measured according to the above-mentioned method.

Adsorption study

Pb^{2+}, Ni^{2+}, Cd^{2+} and Cu^{2+} adsorption capacities of the hydrogel NaAlg-*g*-P(AA-*co*-AM) prepared at a concentration of SDBS equals 1.92 mM (denoted SAP-1.92 mM) were also determined at ambient temperature [37]. For each metal ion, about 0.02 g of the prepared hydrogel sample was accurately weighed into a conical flask and then 200 mL of 100 mg/L of metal ion solution (prepared from metal nitrate salt) was carefully added into the flask. The solutions were stirred at 25 °C for 4 h before it was statically placed for 24 h to allow the metal ion adsorption saturation of the NaAlg-*g*-P(AA-*co*-AM) sample to be achieved. Subsequently, the adsorption solution was filtered and part of the filtrate was diluted to a certain concentration for determination by an atomic absorption spectrometer. Therefore, the metal ion adsorption capacities of NaAlg-*g*-P(AA-*co*-AM) were calculated by Eq. (6).

$$\text{q}(\text{Me}^{2+}) = \frac{(c_0 - c) \times V \times M}{W} \tag{6}$$

where $\text{q}(\text{Me}^{2+})$ is metal ion adsorption capacity of NaAlg-*g*-P(AA-*co*-AM) (mg/g), c_0 and c are the metal ion solution concentrations before and after adsorption (mmol/L), respectively. V is the solution volume (L), M is the atomic molar mass of metal ion (g/mol) and W is the mass of NaAlg-*g*-P(AA-*co*-AM) sample (g).

As for the competitive adsorption: A solution (200 mL) containing 100 mg/L from each metal ion was treated with 0.2 g of hydrogel at 25 °C for 4 h under stirring before it was statically placed for 24 h. After adsorption equilibrium, the concentrations of metal ions in the remaining solution were also evaluated by AAS.

Results and discussions

Preparation and characterization of NaAlg-*g*-P(AA-*co*-AM)

The hydrogels are prepared by free radical polymerization in distilled water under atmospheric condition. Graft polymerization, by an anionic surfactant SDBS micelle templating, of acrylamide (AAm) and acrylic acid (AA) onto sodium alginate is carried out in the presence of MBA as a crosslinking agent, potassium persulfate (KPS) as an initiator and TEMED as a reaction accelerator (Fig. 1). In NaAlg solution, the self-assembly of SDBS can form spherical micelles at a certain concentration of the surfactant. In the process of grafting copolymerization and crosslinking, these micelles may be enclosed in the network and act as a template for pore forming. After removing of SDBS micelles by a washing process, the superabsorbent spongy structure is generated.

FTIR spectra

To investigate the successful grafting of the copolymer onto sodium alginate backbone and removal of SDBS, FTIR spectroscopy was employed.

Figure 2 shows the FTIR spectra of NaAlg, SDBS-free hydrogel, non-washed-SDBS hydrogel, washed hydrogel and SDBS, respectively.

The absorption bands of the NaAlg spectrum (Fig. 2a) at 1616 and 1418 cm^{-1} for the $–COO^-$ shift to 1563 and 1454 cm^{-1}, respectively, in the spectrum of SDBS-free hydrogel (Fig. 2b). The absorption bands at 948 and 889 cm^{-1} of the NaAlg spectrum disappeared in the spectrum of SDBS-free hydrogel while appear the bands at 1170 and 1674 cm^{-1} assigned to $–COO^-$ stretching of acrylate groups and C=O stretching of acrylamide groups, respectively, which suggests the grafting reaction of the copolymer onto sodium alginate backbone [38].

In the spectrum of SDBS-free hydrogel (Fig. 2b) the peaks observed at 3430 and at 3208 cm^{-1} correspond to O–H and N–H stretching, respectively. The peak at 2948 cm^{-1} is assigned to –C–H stretching of the acrylate group. The peaks at 1674 and at 1565 cm^{-1} are assigned to C=O stretching of the acrylamide groups and acrylate groups, respectively [27, 39, 40].

By comparing the FTIR spectra of non-washed-SDBS hydrogel (Fig. 2c) and washed-SDBS-hydrogel (Fig. 2d) the typical peak appearing around 2850 cm^{-1} (the –C–H stretching vibration of $–CH_2–$ of the SDBS molecule) was obviously weakened after the washing process (Fig. 2e) [41].

The O=S=O symmetrical and asymmetrical stretching bands of the sulfonate groups of SDBS molecules appeared at 1186 and 1376 cm^{-1} in non-washed-SDBS

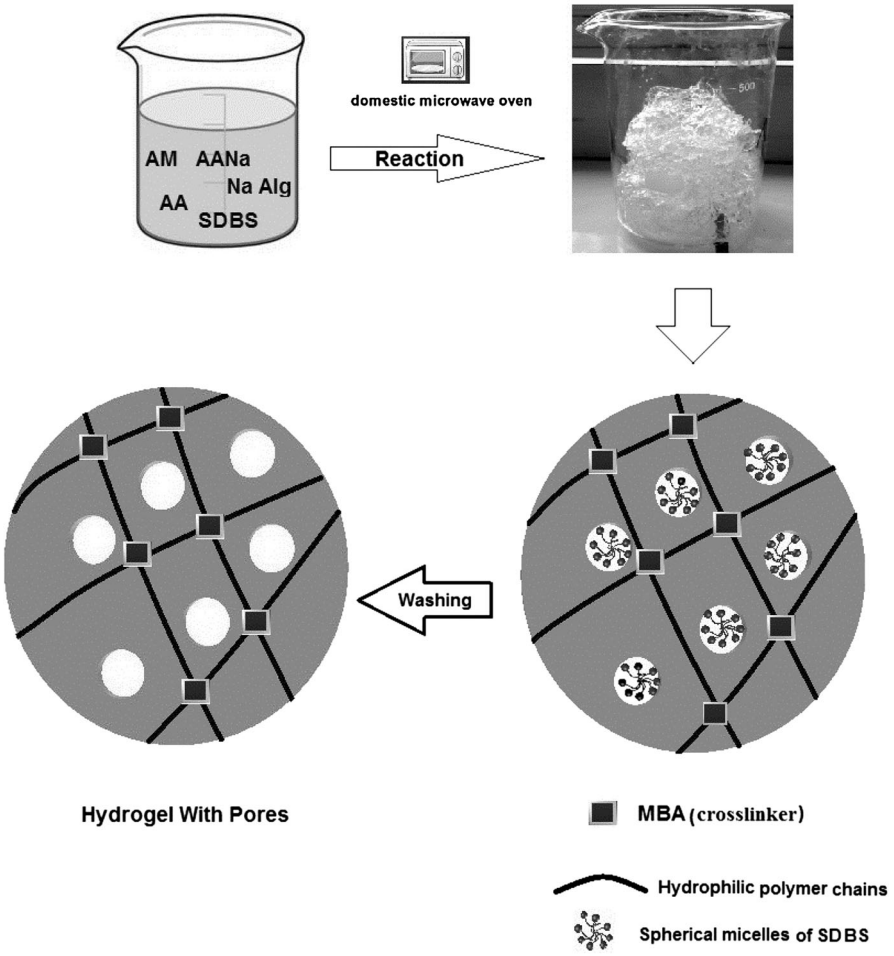

Fig. 1 Proposed reaction scheme for the synthesis of NaAlg-*g*-P(AA-*co*-AM) superabsorbent hydrogel using SDBS micelle templating

hydrogel spectrum and disappeared in the spectrum of washed-SDBS hydrogel [42, 43].

Furthermore, the characteristic absorption peaks for SDBS-free and washed-SDBS hydrogel are identical, which infers that all residual SDBS has been removed from the hydrogel network, (Fig. 2b, d).

X-ray patterns

The X-ray powder diffraction patterns of alginate, copolymer and alginate grafted copolymers are illustrated in Fig. 3. Compared with the original alginate, grafted copolymer shows a weaker and broader peak in the $2\theta = 17°–37°$ region, which

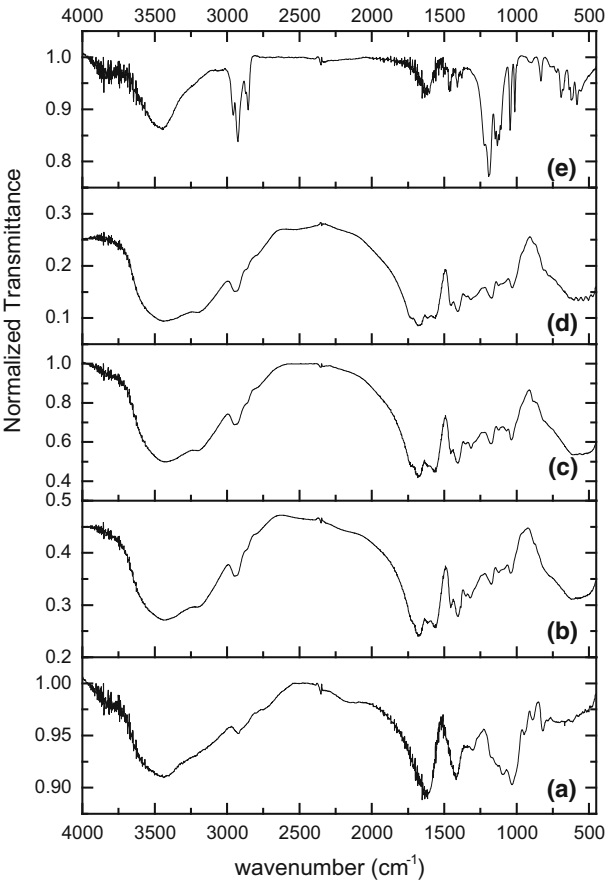

Fig. 2 FTIR spectra of *a* NaAlg, *b* SDBS-free hydrogel, *c* non-washed-SDBS hydrogel, *d* washed hydrogel, and *e* SDBS

demonstrates that the grafting suppressed the partial crystallization of alginate to some extent. It is also suggested that the NaAlg and copolymer are mixed well at the molecular level.

Thermogravimetric analysis

Thermogravimetric degradation curves of the NaAlg and NaAlg-*g*-P(AA-*co*-AM) in argon atmosphere are displayed in Fig. 4. NaAlg thermogram exhibits two-step degradation behavior. The one in the range 20–180 °C is ascribed to the elimination of free water adsorbed to the hydrophilic polymer. The other in the range 200–300 °C is assigned to a complex process including dehydration of the saccharide rings, depolymerization with the formation of water, CO_2 and CH_4 as reported in the literature [44]. The temperature of 50 % weight loss is at 281.02 °C.

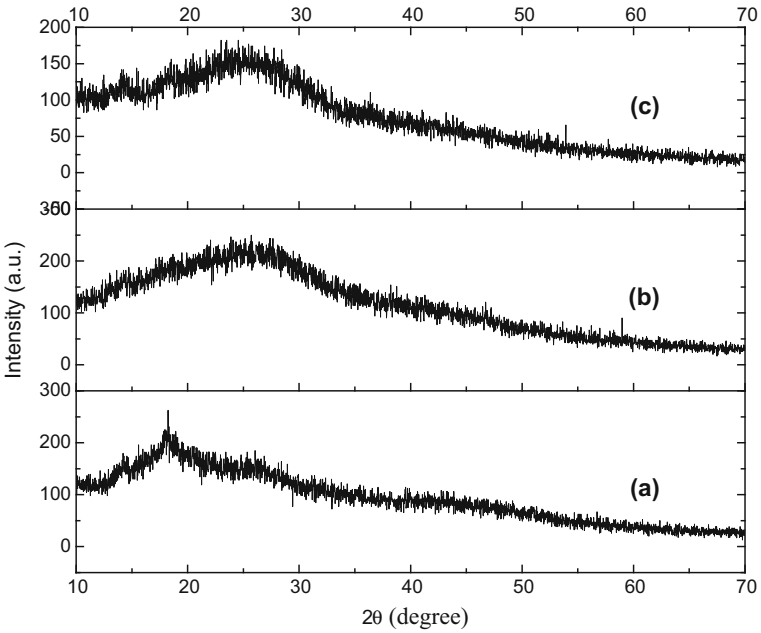

Fig. 3 X-ray diffraction patterns of *a* NaAlg, *b* P(AA-*co*-AM) and *c* NaAlg-*g*-P(AA-*co*-AM)

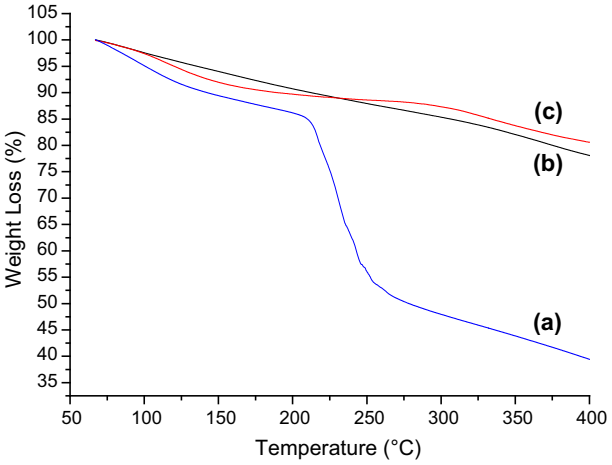

Fig. 4 TG curves of *a* NaAlg, *b* NaAlg-*g*-P(AA-*co*-AM) and *c* P(AA-*co*-AM)

At that temperature, the grafted hydrogel NaAlg-*g*-P(AA-*co*-AM) and the copolymer P(AA-*co*-AM) exhibit weight losses of 14.07 and 11.71 %, respectively.

From the TG curves, it can be concluded that the grafting of P(AA-co-AM) onto NaAlg backbone enhances the thermal stability of the polysaccharide, which can indicate that the grafted hydrogel was synthesized successfully. This phenomenon

has been reported by Işiklan and Küçükbalcı [44]. They have indicated that grafting poly(N-isopropylacrylamide) onto alginate improved the thermal stability of the natural polymer.

Morphological analyses

To study the change of surface morphology of the SAPs resulting from the introduction micelles templating using SDBS, SEM micrographs of NaAlg-*g*-P(AA-*co*-AM) with different SDBS concentrations were observed and are shown in Fig. 5.

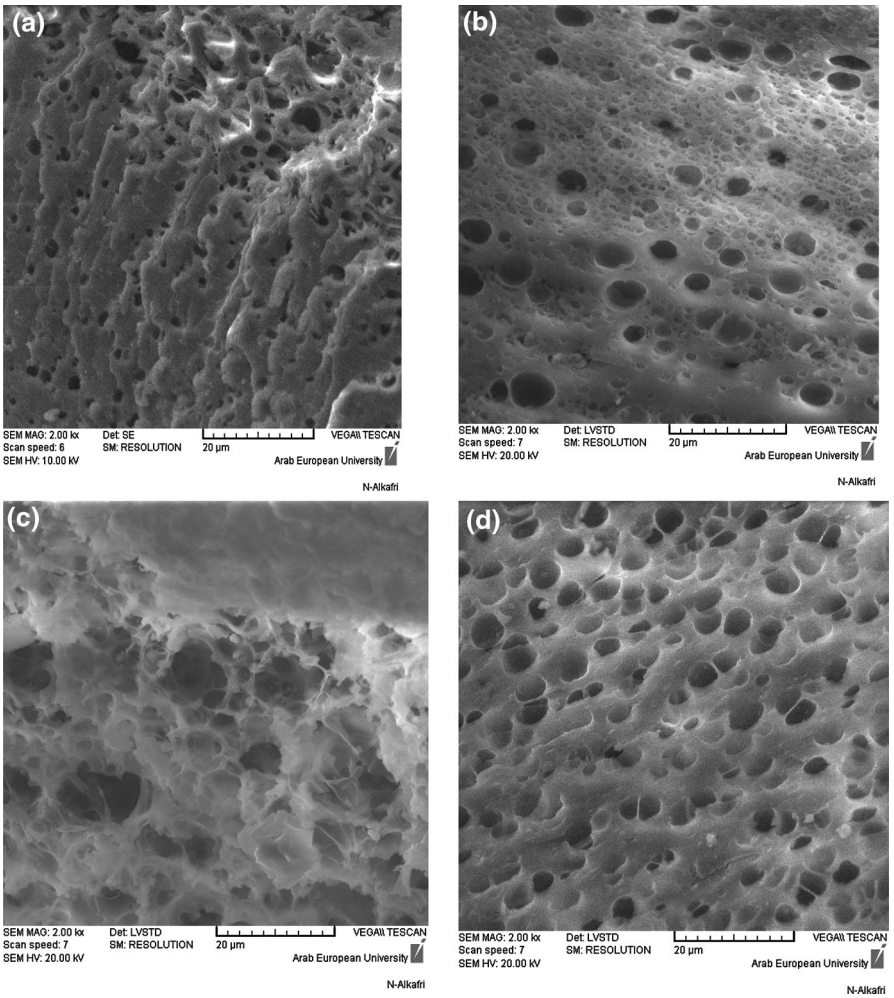

Fig. 5 SEM micrographs of SAP with different concentrations of SDBS **a** 0 mM, **b** 0.96 mM, **c** 1.92 mM, and **d** 3.84 mM at the same magnification scale

The SEM micrograph of SDBS-free SAP has a relatively compact structure with an average pore size of 3.288 μm. But the structure has not interconnected open cellular structure (Fig. 5a). The average size of pores increases with increasing the content of SBDS (Fig. 5b–d). This could be attributed to the self assembling of SDBS molecules in the reactive medium and the micelles acting as a pore-forming templating. We clearly notice that the sample with SDBS concentration 1.92 mM presents an average diameter pore of 8.28 μm with an interconnected open cellular structure (Fig. 6). This could be linked to the formation of a superporous structure [45].

Further increase in SDBS concentration (concentration of 3.84 mM) results in a more fragile and easy to collapse porous structure. According to Su et al. [46], micelle formation at higher concentration of SDBS could interfere with the gellation process (Fig. 5d).

Effect of SDBS concentration on the swelling ratio and swelling kinetics

It is well established that the porosity of the hydrogel has great effect on water absorbency [7]. According to morphological studies, we have proven that the pore size of the prepared hydrogels depends on the concentration of the surfactant SDBS. Figure 7 depicts the variation of the absorbency of the hydrogels with different concentrations of SDBS as a function of time. For each kinetic curve, we can distinguish two sections: the initial rapid increase and the stabilized equilibrium absorbency (S_{eq}). The asymptotic value S_{eq} is dependent on SDBS concentration. The highest value of S_{eq} corresponds to a concentration of 1.92 mM of SDBS. This result is in perfect coherence with the morphological studies, as the microstructure of this hydrogel has higher pore sizes and exhibits an interconnected open cellular structure compared with the other hydrogels. To study the effect of SDBS on the absorbency we used the pseudo second-order swelling kinetic model proposed by Schott [47]:

$$\frac{t}{S_w} = \frac{1}{k_{it}} + \frac{1}{S_\infty} t \tag{7}$$

where S_w is the swelling ratio at time t, S_∞ is the theoretical equilibrium swelling ratio and k_{it} is the initial swelling rate constant. According to Fig. 8 the plots of the average swelling rate (t/S_w) versus swelling time (t) give straight lines $(R^2 > 0.999)$, indicating that the swelling process follows pseudo second-order swelling kinetic model. k_{it} and S_∞ values can be calculated through the slope and intercept of the fitted straight lines (Figs. 9, 10). It is clearly seen that the theoretical S_∞ presents similar tendency as S_{eq} when changing SDBS concentration. Moreover, the initial swelling rate constant k_{it} also increases with increasing SDBS concentration from 0 to 1.92 mM and then it decreases with further increase of SDBS concentration. In fact, the more porous is the gel, the more is the specific surface area and the faster is water diffusion into the gel. This leads to an improved initial swelling rate. Furthermore, the k_{it} values for different SDBS concentrations imply

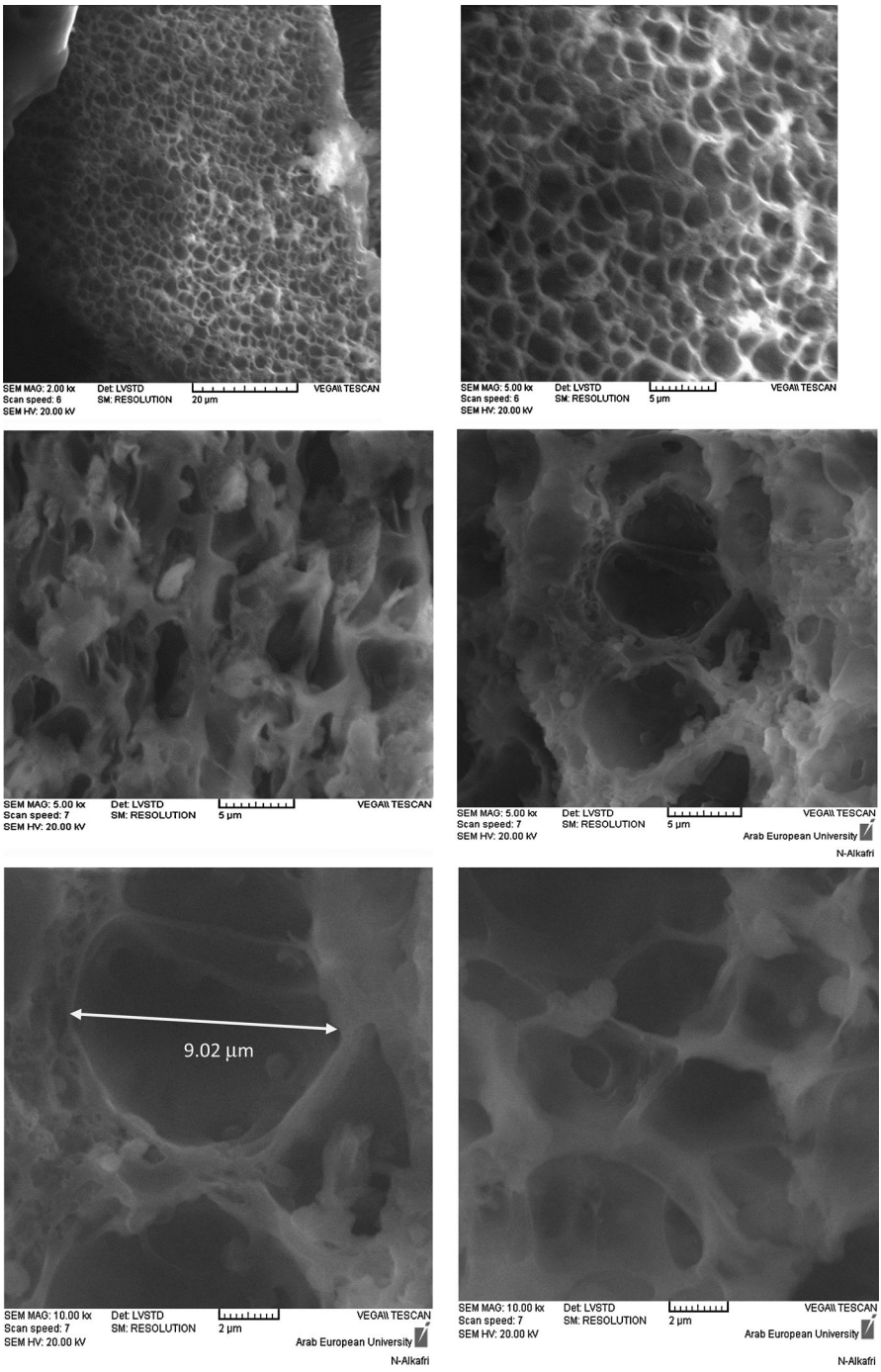

Fig. 6 SEM micrographs of SAP at the concentration of SDBS 1.92 mM with different magnifications

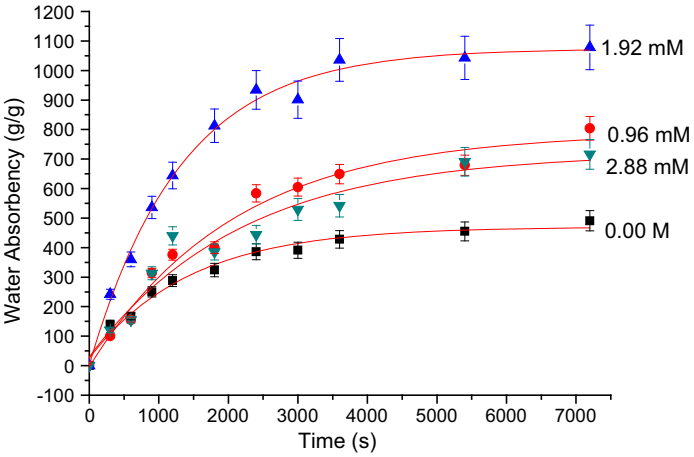

Fig. 7 Time-dependent swelling curves of the SAPs generated by different concentrations of SDBS in distilled water

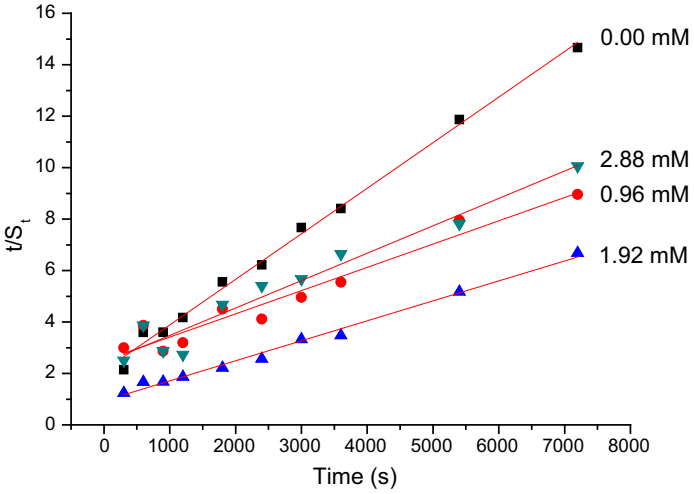

Fig. 8 The t/S_w versus t graphs according to Schott's pseudo second-order swelling kinetics model

that the hydrogel prepared with a concentration of SDBS equals to 1.92 mM has the best microstructure that promotes the swelling rate.

The key result of the current study is that there is an optimum concentration, 1.92 mM of SDBS. At this concentration, the swelling rate and swelling ratio have the highest values. This optimum concentration is the same as the one found when studying the morphology of the prepared gels. At this optimum concentration, SDBS molecules self-assemble and the micelles act as a pore-forming templating. The hydrogel has then higher pore sizes and exhibits an interconnected open cellular

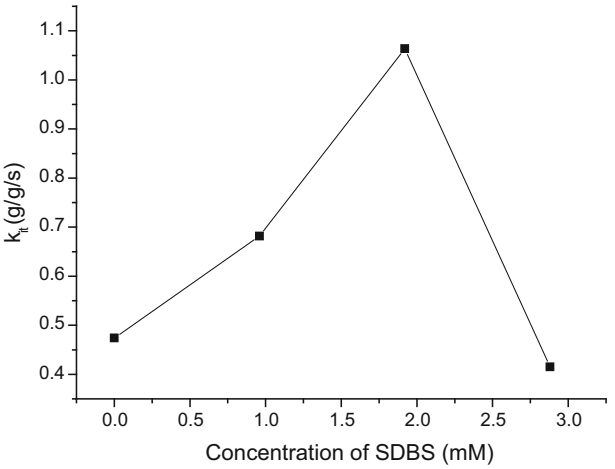

Fig. 9 Variation of the initial swelling rate constant (k_{it}) with different SDBS concentrations

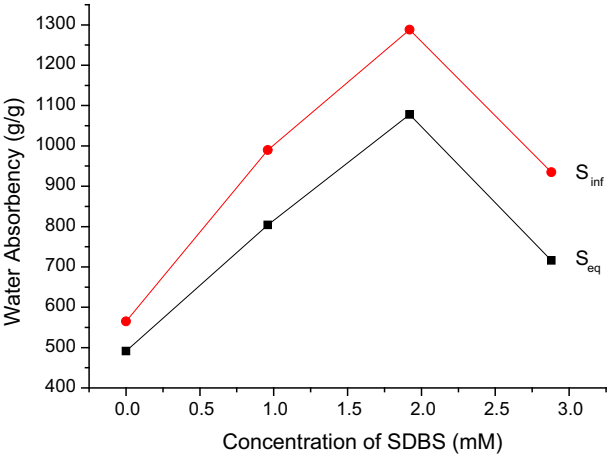

Fig. 10 Variation of theoretical equilibrium swelling (S_∞) with different SDBS concentrations

structure which is reflected on the swelling behavior of the hydrogel by the highest initial swelling rate and excellent swelling capacity.

Water retention

Table 1 presents the variation of water retention with varying SDBS concentration (mM).

It can be concluded that the anionic surfactant templating has a benefic effect in enhancing water retention as the SDBS-free hydrogel has only about 73 % of water

Table 1 Variation of water retention, gel content, grafting percentage and grafting efficiency with varying SDBS concentration (mM)

SDBS concentration (mM)	0.00	0.96	1.92	3.84
Water retention (%)	73.6	82.3	81.5	82.7
Gel content (%)	72	62	75	70
Grafting percentage (G %)	704.8	596.5	746.7	698.2
Grafting efficiency (E %)	70.5	59.7	74.7	69.8

retention compared to about 81 % for the others hydrogel. This could be attributed to more water captured in a more porous structure.

Gel content, grafting percentage and grafting efficiency

Table 1 also presents the variation of gel content, grafting percentage and grafting efficiency with varying SDBS concentration (mM). As clearly seen in Table 1, these parameters strongly depend on surfactant concentration indicating the interference of micelle formation with the gellation and grafting processes. Furthermore, the values of gel content, grafting efficiency and grafting percentage are the highest when the concentration is 1.92 mM of SDBS. This concentration is the optimum one found when discussing the swelling kinetics and the morphology of the synthesized gels. This result confirms our assumption of the presence of an optimum SDBS for micelle formation.

Effect of the environmental parameters on water absorbency

Effects of salt solution on water absorbency

The optimized SAP was tested for the effect of water salinity on its swelling capacity.

Different concentrations of NaCl, $MgCl_2$, $AlCl_3$ solutions were prepared to study the effect of ion charge and ion concentration on water absorption. The absorbency of the synthesized hydrogel was measured by the same procedure adopted above in the case of distilled water.

Figure 11 shows that water absorption decreases with increasing the ionic strength of the saline solution as cited in Flory equation [48]. The ionic strength of the solution depends on both the concentration and the charge of each individual ion. In fact, the presence of ions in the solution decreases the osmotic pressure difference, the driving force for the swelling between the gel and the solution. In addition, multivalent cations (Mg^{2+} and Al^{3+}) can neutralize several charges inside the gel by complex formation with carboxamide or carboxylate groups, leading to increased ionic crosslinking degree and consequently loss of swelling. The effect of cation charge and its concentration on swelling can be concluded from (Fig. 11).

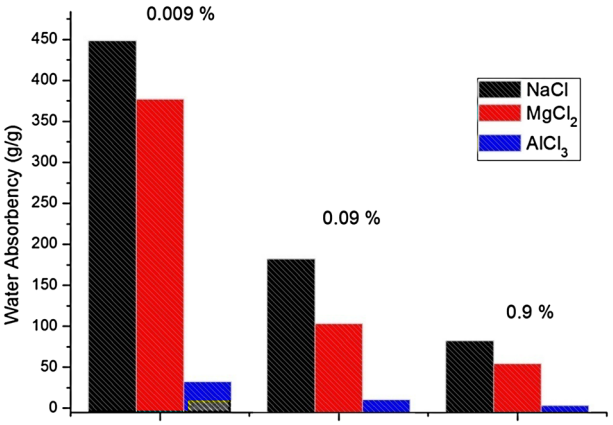

Fig. 11 Histogram of variation of water absorbency of SAP with different ion charge and ion concentration of saline solutions

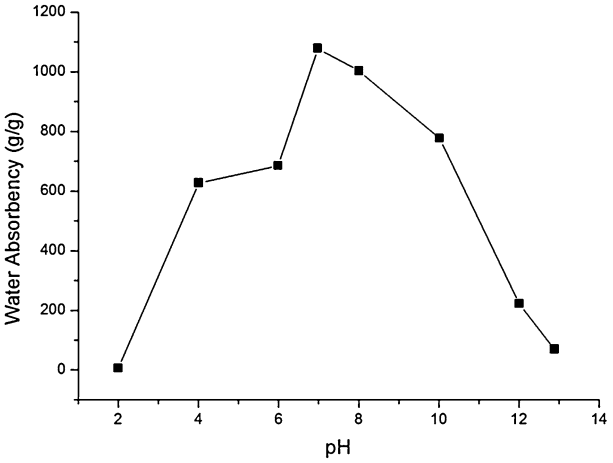

Fig. 12 Effect of environmental pH on water absorbency

Effect of pH on water absorbency and pH responsive characteristics

Studies have indicated that water absorption of hydrogels is sensitive to environmental pH [49]. So, the swelling behavior of synthesized SAP was studied at various pH value between 2.0 and 13.0, at room temperature (Fig. 12). Since the swelling capacity of all "anionic" hydrogels is appreciably decreased by addition of counter ions to the swelling medium, no buffer solutions were used when studying the net effect of pH on water absorbency. Therefore, a stock of concentrated solution HCl and NaOH was diluted with distilled water to reach the desired acidic or basic pH [50].

The absorbency of the synthesized hydrogel was measured by the same procedure adopted above in the case of distilled water.

It can be clearly observed that the SAP almost does not swell at pH 2, but it sharply swells as increasing external pH values. We can explain the variation of absorbency with variation of pH as follows:

As anionic polymer, the SAP prepared using micelle templating formed by the self-assembled anionic surfactant SDBS contains numerous hydrophilic $–COO^-$, –COOH and NH_2 groups. At low pH, sodium carboxylate group on the polymer network is protonated. On one hand, the hydrogen-bonding interaction among –COOH and NH_2 groups was strengthened and the additional physical crosslinking was generated. On the other hand, the electrostatic repulsion among $–COO^-$ groups was restricted, and so the SAP network tends to shrink, and becomes hydrophobe [25]. In the interval pH 4–8, some of carboxylic acid groups are ionized and the electrostatic repulsion between $–COO^-$ groups causes an enhancement of the swelling capacity [27].

At high pH, the swelling capacity also decreases by "charge screening effect" of excess Na^+ in the swelling media, which shields the carboxylate anions and prevent effective anion–anion repulsion [27].

The evidence change of water absorption with altering the pH of external solution confirms the excellent pH-sensitivity behavior of the prepared SDBS-hydrogels.

We have also studied the swelling kinetics of the SAP at different pH values (Fig. 13). As can be seen, the swelling kinetics of the SAP is dependent on the pH values of the swelling medium.

The time-dependency of the swelling behavior of SDBS-1.92 mM hydrogel is studied for different pH values (Fig. 13). We used solutions of HCl (pH 1.0) and NaOH (pH 13.0) to adjust the pH value of the studied solution and to avoid the influence of ionic strength. Figures 13 and 14 depict clearly the swelling kinetics of

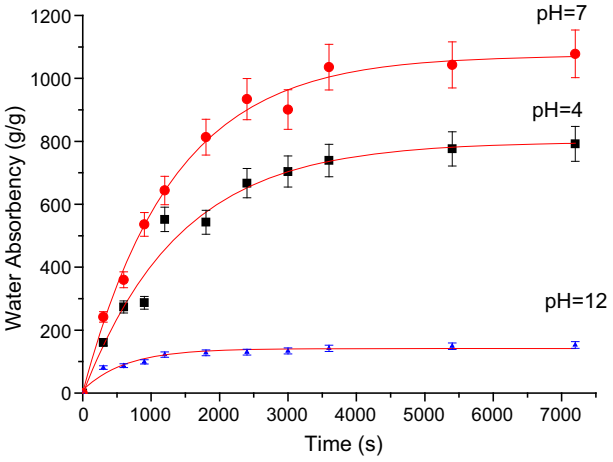

Fig. 13 Swelling kinetics at different pH values

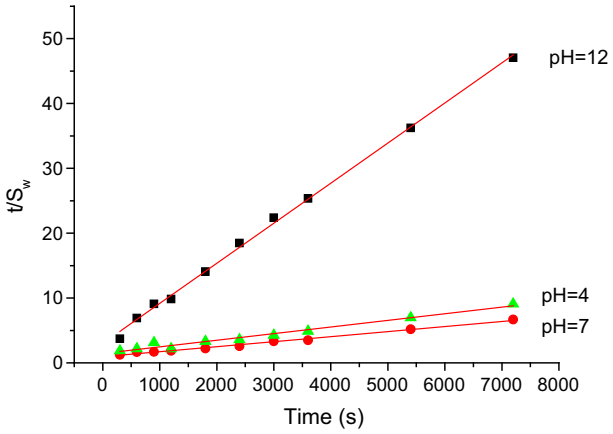

Fig. 14 Schott's pseudo second-order swelling kinetics model for pH kinetics study

the SAP as a function of the pH values. To determine the swelling kinetic parameters (k_{it} and S_∞) in various pH solutions we used the Schott's pseudo second-order kinetics model (Eq. 5). According to (Fig. 14) the plots of the average swelling rate (t/S_w) versus swelling time (t) give straight lines $(R^2 > 0.997)$, indicating that the swelling process follows pseudo second-order swelling kinetic model. k_{it} and S_∞ values can be calculated through the slope and intercept of the fitted straight lines. The k_{it} values for pH values 4.0, 7.0 and 12.0 are, respectively, 0.687, 1.063 and 0.335 g/(g s). S_∞ values are 980, 1288 and 162 g/g, respectively. The S_{eq} (792, 1078, 153 g/g) and S_∞ are almost equal which suggests that the swelling behavior of the SAP at different pH solutions could reach about 84 % of its equilibrium absorbency within 2 h. The change tendency of k_{it} as a function of pH values is similar with S_∞. The initial swelling rate of the SAP is related to the relaxation rate of the chain segments in the network. The ionization of carboxylate groups occurs at pH >4.7 and this trend is increased at higher pH. On the other hand, the increased carboxylate groups lead to a stronger electrostatic repulsion, which is benefic to the relaxation of the polymer network. The fast relaxation is favorable to the penetration of water molecules into the gel network more easily, and so the initial swelling rate can be enhanced. But at higher pH >10, the mobility of polymer network is reduced by the screening effect of cations which limits the diffusion of water molecules into the polymer network, and consequently the initial swelling rate is decreased.

Since the SAPs show different swelling behaviors at various pH values, we investigated their pH reversibility in aqueous solutions adjusted at pH values 2.0 and 7.0, respectively. Figure 15 shows a stepwise reproducible swelling change of the SAP at 25 °C with alternating pH between 2.0 and 7.0. The time interval between the pH changes was 15 min. At pH 7.0 the hydrogel swells due to anion–anion repulsive electrostatic forces, while at pH 2.0, it shrinks within a few minutes due to protonation of carboxylate groups. This sharp swelling–deswelling behavior of the SAPs makes them suitable candidates for controlled releasing systems.

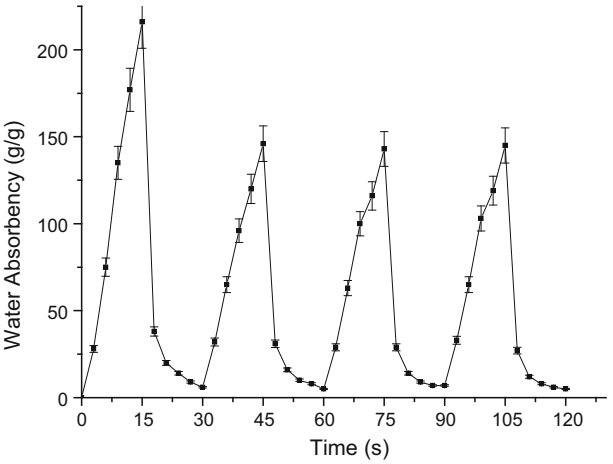

Fig. 15 Swelling–deswelling behavior of the SAP between pH values 7.0 and 2.0, respectively. The time interval between the pH changes was 15 min

Adsorption of heavy metal ions on the SAP

Single and multi-element aqueous solutions

Table 2 shows adsorption capacities of Pb(II), Cd(II), Ni(II) and Cu(II) on SDBS-1.92 mM hydrogel in single and multi-element aqueous solutions.

The adsorption capacities of SAP-1.92 mM are 231.88, 235.62, 67.52 and 76.35 mg/g for Pb(II), Cd(II), Ni(II) and Cu(II), respectively. The affinity order (weight based) is Cd(II) > Pb(II) > Cu(II) > Ni(II).

As wastewater often contains more than one heavy metal species, it is possible that the behavior of particular metal specie is affected by the presence of other metals. So, competitive adsorption of heavy metal ions from their mixture was also investigated. The adsorption capacities diminish, Table 2. This decrease is expected due to the increased ionic strength of the aqueous solution. The affinity order (weight based) is Pb(II) > Cu(II) > Cd(II) > Ni(II).

Table 2 Adsorption capacities of Pb(II), Cd(II), Ni(II) and Cu(II) on SAP-1.92 mM (0.02 g hydrogel) in single and multi-element aqueous solutions

Metal ion	Pb(II)	Cd(II)	Ni(II)	Cu(II)
q(Me^{2+}) (mg/g)	231.88	235.62	67.52	76.35
q(Me^{2+}) (μmol/g)	1119	2096	1150	1201
q(Me^{2+}) (mg/g) competitive adsorption	120.04	31.18	6.720	67.99
q(Me^{2+}) (μmol/g) competitive adsorption	579	277	115	1070

Table 3 Effect of initial heavy metal ion concentration on the adsorption capacity on SAP-1.92 mM (0.01 g hydrogel)

Metal ion Pb(II) ($mg.L^{-1}$)	50	100	200	300
Amount of the sorbed metal ion (mg/g)	244.83	360.93	366.61	471.99

Effect of initial heavy metal ion concentration

The effect of initial heavy ion concentration on the adsorption capacity was investigated on lead ion Pb(II), Table 3. Adsorption capacity increased from 244.83 mg/g for 50 mg/L initial lead ion concentration to 471.99 mg/g for 300 mg/L initial lead ion concentration. This result is related to a greater driving force for mass transfer of lead ion from solution to solid surface at higher concentrations.

Adsorption isotherms

Langmuir and Freundlich models are two common isotherm models that are used to determine the affinity of sorbent and adsorbate and to find the mechanism of adsorption. In Langmuir model, adsorption occurs as a monolayer process on homogeneous and energetically equivalent sites, while in Freundlich model, adsorption is a multilayer process and adsorbent surface is heterogeneous and energetically non-equivalent. Langmuir and Freundlich isotherm models are expressed as Eqs. (8) and (9), respectively [37, 51].

$$\frac{C_{\mathrm{eq}}}{q} = \frac{1}{bQ_{\max}} + \frac{C_{\mathrm{eq}}}{Q_{\max}} \tag{8}$$

$$\log\, q = \log\, K_F + \frac{1}{n}\log\, C_{\mathrm{eq}} \tag{9}$$

where q is the concentration of the adsorbed metal ion on the adsorbent (mg g^{-1}), C_{eq} is the equilibrium metal ion concentration in solution (mg L^{-1}), b is the Langmuir constant (L mg^{-1}), and $Q_{\max}$ is the maximum adsorption capacity (mg g^{-1}), K_F is Freundlich constant (mg g^{-1}) and n is heterogeneity factor.

Table 4 lists the constants calculated from the plot of the two models for Pb(II). As it is shown in this table, the correlation coefficient (R^2) for Langmuir isotherm model is higher than that of Freundlich model, indicating that adsorption of metal ion is better described by Langmuir isotherm model. Maximum adsorption capacity ($q_{\max} = 480.77$ mg/g) predicted by this model is in good agreement with the value obtained experimentally 471.99 mg/g.

The value of free energy change (ΔG^0) for the sorption process is calculated, using the following Eq. (10), [51]:

$$\Delta G^0 = -RT \ln b \tag{10}$$

The estimated value of ΔG^0 for adsorption of Pb(II) onto SAP was -23.14kJ mol^{-1}. Negative ΔG^0 indicates the spontaneous nature of the adsorption process.

Table 4 Adsorption constants for the sorption of Pb(II) on SAP-1.92 mM (0.01 g hydrogel)

Freundlich constants			Langmuir constants				ΔG^0kJ mol^{-1}
K_F	n	R_F^2	Q_m(mg g^{-1})	b(L mg^{-1})	b(L mol^{-1})	R_L^2	
147.13	4.75	0.7871	480.77	0.0547	11,333.84	0.9471	−23.14

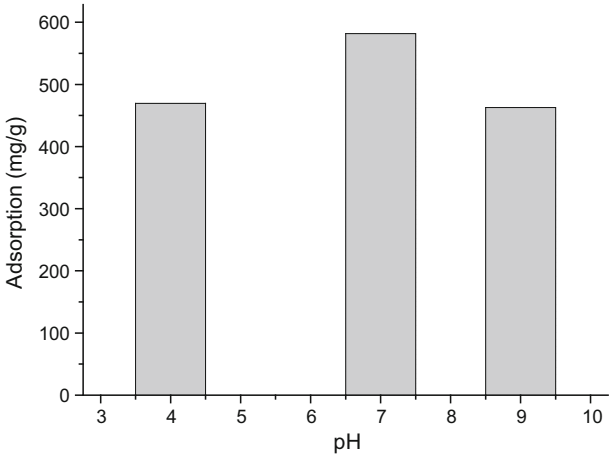

Fig. 16 Adsorption of lead ion at different pH values on SAP-1.92 mM (0.02 g hydrogel)

Effect of initial pH

Figure 16 depicts the effect of pH values of solution on the adsorption capacity of SAP-1.92 mM for lead ion Pb(II). The initial concentrations of Pb(II) solution are 100 mg/L. The mass of SAP is about 0.02 g weighed accurately and immersed in 200 mL of pH solution. The adsorption time was set at 24 h. As seen from Fig. 16, the adsorption capacity reaches a maximum at pH 7. In fact, when pH is $4 < \text{pH} < 8$, some of carboxylic acid groups are ionized and the electrostatic repulsion between carboxylate groups causes an enhancement of the swelling capacity. This result is in good agreement with that found when discussing the effect of environmental pH on water absorbency.

Desorption and reusability of SAP

The results above show that SAP-1.92 mM exhibits excellent adsorption capabilities for hazardous lead ion. But for economic and environmental point of view, it is necessary that such adsorbent material is able to be used repeatedly.

Desorption of Pb(II) is achieved on samples of 0.01 g of SAP-1.92 mM loaded by different amounts of Pb(II). They were stirred with HNO_3 solution—as a desorption agent—(50 mL, 0.1 M) at 25 °C for 150 min. The final metal ion

Table 5 Adsorption–desorption values of Pb(II) after three consecutive cycles of adsorption and desorption on SAP-1.92 mM (0.01 g hydrogel)

Amount of Pb(II) (mg/g) loaded	244.83	360.93	366.61	471.99
Amount of the desorbed Pb(II) (mg/g)	211.75	299.20	300.00	417.00
Desorption ratio (%)	86.49	82.90	81.83	88.35

concentration in the aqueous phase was determined using AAS. The desorption ratio was calculated from the Eq. (11):

$$\text{Desorption ratio } \% = \frac{\text{Amount of metal ions desorbed (mg)}}{\text{Amount of metal ion adsorbed onto the SAP}} \times 100 \quad (11)$$

To determine their reusability, the desorbed hydrogels are regenerated with 0.1 mol/L NaOH for 30 min and then used for another adsorption.

The cycles of adsorption–desorption were repeated three times. Table 5 shows the adsorption–desorption values of Pb(II) after three consecutive cycles of adsorption and desorption. The desorption ratios vary between 81.83 and 88.35 %. Although the amount of ion adsorption decreases after regeneration, however, the hydrogel maintained nearly 85 % of their original adsorption capacity after three consecutive cycles of adsorption and desorption. This result suggests that the SAP-1.92 mM is a potential candidate for the design of a continuous sorption process.

Conclusion

In this work we succeeded, using microwave irradiation, to prepare a new SAPs with porous structure by the grafting copolymer P(AA-*co*-AM) onto the backbone of a renewable and biodegradable substrate of sodium alginate in the presence of redox couple initiator of KPS/TEMED and crosslinker MBA, using the self-assembled SDBS micelles as a pore-forming templating.

The method of preparation is fast and simple. It does not need the use of an inert gas during synthesis. FTIR analysis confirmed that the copolymer P(AA-*co*-AM) chains had been grafted onto the macromolecular chains of NaAlg, and SDBS was removed from the final product during washing process.

The SDBS concentration strongly affects the morphology and the pore structure as demonstrated by SEM results. There is an optimum concentration of SDBD (1.92 mM) at which SDBS molecules self-assemble and the micelles act as a pore-forming templating. At this concentration the hydrogel has a well-defined pore structure and higher pore sizes and exhibits an interconnected open cellular structure. This is reflected on the swelling behavior of the hydrogel by a high initial swelling rate (63.84 g g^{-1} min^{-1}) and a high swelling capacity (1078 g/g).

The special porous sponge structure has endowed NaAlg-*g*-P(AA-*co*-AM) hydrogel with a high adsorption capacity for metal ions. Adsorption of Pb(II) is better described by Langmuir isotherm model and maximum adsorption capacity up to 480.77 mg. g^{-1} is obtained. Adsorption capacity is dependent on pH values and

is increased by increasing the initial metal ion concentration. The adsorbent exhibits high removal efficiency after three cycles of adsorption. Adsorption capacity of the optimized hydrogel for other hazardous heavy metal ions Cd(II), Ni(II) and Cu(II) and their competitive adsorption are also investigated. The results indicate that the optimized hydrogel offers a cheap and efficient removing agent for hazardous heavy metal ions form wastewater.

References

1. Shi Y, Xue Z, Wang X, Wang L, Wang A (2013) Removal of methylene blue from aqueous solution by sorption on lignocelluloses–g-poly(acrylic acid)/montmorillonite three-dimensional cross-linked polymeric network hydrogels. Polym Bull 70:1163–1179
2. Dubrovskii SA, Afanas'eva MV, Lagutina MA, Kazanskii KS (1990) Comprehensive characterization of superabsorbent polymers hydrogels. Polym Bull 24:107–113
3. Shi X, Wang W, Wang A (2011) Effect of surfactant on porosity and swelling behaviors of guar gum-g-poly(sodium acrylate-co-styrene)/attapulgite superabsorbent hydrogels. Colloid Surf B
4. Kuang J, Yuk KY, Huh KM (2011) Polysaccharide-based superporous hydrogels with fast swelling and superabsorbent properties. Carbohydr Polym 83(1):284–290
5. Lee WF, Wum RJ (1996) Superabsorbent materials. 1. Swelling behaviors of crosslinked poly(-sodium acrylate-co- hydroxyethyl methacrylate) in aqueous salt solution. J Appl Polym Sci 62(7):1099–1114
6. Li W, Wang JL, Zou LZ, Zhu SQ (2008) Syhthesis and characterization of the thermo- and pH-sensitive hydrogels and microporous hydrogel induced by the NP-10 aqeous two-phase system. Eur Polym J 44:3688–3699
7. Shi X, Wang W, Wang A (2013) pH- responsive sodium alginate-based superporous hydrogel generated by an anionic surfactant micelle templating. Carbohyd Polym 94:449–455
8. Poursamara SA, Azamib M, Mozafari M (2011) Controllable synthesis and characterization of porous polyvinyl alcohol/hydroxyapatite nanocomposite scaffolfs via an in situ colloidal technique. Colloid Surf B Biointerfaces 84:310–316
9. Park H, Kim D (2006) Swelling and mechanical properties of glycol chitosan/poly(vinyl alcohol) IPN-type superporous hydrogels. J Boimed Mater Res Part A 78A:662–667
10. Delaney JT, Liberski AR, Perelaer J, Schubert US (2010) Reactive inkjet printing of calcum alginate hydrogel porogens-A new strategy to open-pore structure matrices with controlled geometry. Soft Matter 6:866–869
11. Elbert DL (2011) Liquid- liquid two-phase systems for the production of porous hydrogels and hydrogel microspheres for biomedical application: a tutorial review. Acta Biomater 7:31–56
12. Partrap S, Muthutantri A, Rehman IU, Davis GR, Darr JA (2007) Preparation and charactriation of controlled porosity alginate hydrogels made via a simultaneous micelle templating and internal gelation process. J Mater Sci 42:3502–3507
13. Shi X, Tangjie, Wang A (2015) Develpoment of a superporous hydroxyethyl cellulose—based hydrogel by anionic surfactant micelle templating with fast swelling and superabsorbent properties. J Appl Polym Sci 42027–42034
14. Lee EA, Balakrishnan P, Song CK, Choi JH, Noh GY, Park CG et al (2010) Microemulsion-based hydrogel formulation of itraconazole for topical delivery. J Pharm Investig 40:305–311
15. Ji CD, Khademhosseini A, Dehghani F (2011) Enhancing cell penetration and proliferation in chitosan hydrogels for tissue engineering applications. Biomater 32:9719–9729
16. Chatterjee S, Chatterjee T, Woo SH (2010) A new type of chitosan hydrogel sorbent generated by anionic surfactant gelation. Bioresour Technol 101:3853–3858
17. Reddy KR, Gomes VG, Hassan M (2014) Carbon functionalized TiO_2 nanofibers for high efficiency photocatalysis. Mater Res Express 1(015012):1–15
18. Reddy KR, Hassan M, Gomes VG (2015) Hybrid nanostructures based on titanium dioxide for enhanced photocatalysis. Appl Catalys A Gen 489:1–16

19. Reddy KR, Nakata K, Ochiai T, Murakami T, Tryk DA, Fujishima A (2011) Facile fabrication and photocatalytic application of Ag nanoparticles-TiO_2 nanofiber composites. J Nanosci Nanotech 11(4):3692–3695
20. Huang SY, Fan CS, Hou CH (2014) Electro-enhanced removal of copper ions from aqueous solutions by capacitive deionization. J Hazard Mater 278:8–15
21. Showkat AM, Zhang YP, Kim MS, Gopalan AI, Reddy KR, Lee KP (2007) Analysis of heavy metal toxic ions by adsorption onto amino-functionalized ordered mesoporous silica. Bull Kor Chem Soc 28(11):1985–1992
22. Zhu Y, Zheng Y, Wang A (2015) A simple approche to fabricate granular adsorbent for adsorption of rare elements. Int J Biolog Macromol 72:410–420
23. Zhu Y, Zheng Y, Wang A (2014) Preparation of granular hydrogel composite by the redox couple for efficient and fast adsorption of La(III) and Ce(III). J Environ Chem Eng 3(2):1416–1425
24. Zheng Y, Zhu Y, Wang A (2014) Highly efficient and selective adsorption of malachite green onto granular composite hydrogel. Chem Eng J 257:66–73
25. Wang W, Wang A (2010) Synthesis and swelling properties of pH-sensitive semi-IPN superabsorbent hydrogels based on sodium alginate-g-poly(sodium acrylate) and polyvinylpyrrolidone. Carbohyd Polym 80:1028–1036
26. Yiğitoğlu M, Aydin G, Işiklan N (2014) Microwave-assisted synthesis of alginate-g-polyvinylpyrrolidone copolymer and its application in controlled drug release. Polym Bull 71:385–414
27. Kalaleh HA, Tally M, Atassi Y (2013) Preparation of a clay based superabsorbent polymer composite of copolymer poly(acrylate-co-acrylamide) with bentonite via microwave radiation. Res Rev Polym 4:145–150
28. Tally M, Atassi Y (2015) Optimized Synthesis and swelling properties of a pH-sensitive semi-IPN superabsorbent polymer based on sodium alginate-*g*-poly(acrylic acid-co-acrylamide) and polyvinylpyrrolidone and obtained via microwave irradiation. J Polym Res 22(9):1–13
29. Kalaleh HA, Tally M, Atassi Y (2015) Optimization of the preparation of bentonite-*g*-poly(acrylate-co-acrylamide) superabsorbent polymer composite for agricultural applications. Polym Sci Ser B 57(6)
30. Zohuriaan-Mehr MJ, Kabiri K (2008) Superabsorbent polymers materials: a review. Iran Polym J 17:451–477
31. El-Sayed M, Sorour M, Abd ElMoneem N, Talaat H, Shalaan H, ElMarsafy S (2011) Synthesis and properties of natural polymers—grafted-acrylamide. World Appl Sci J 13:360–368
32. Ghasemzadeh H, Ghanaat F (2014) Antimicrobial alginate/PVA silver nanocomposite hydrogel, synthesis and characterization. J Polym Res 21:355–368
33. Jeng YT (2015) Preparation and characterization of controlled release fertilizers using alginate-based superabsorbent polymer for plantations in Malaysia. Master thesis, University Tunku Abdul Rahman, Malaysia
34. Rashidzadeh A, Olad A, Salari D, Reyhanitabar A (2014) On the preparation and swelling properties of hydrogel nanocomposite based on sodium alginate-*g*-poly(acrylic acid-co-acrylamide)/clinoptilolite and its application as slow release fertilizer. J Polym Res 21:344–359
35. Huang M, Shen X, Sheng Y, Fang Y (2005) Study of graft copolymerization of *N*-maleamic acid-chitosan and butyl acrylate by gamma-ray irradiation. Int J Biol Macromol 36:98–102
36. Bao Y, Ma J, Li N (2011) Synthesis and swelling behaviors of sodium carboxymethyl cellulose-*g*-poly(AA-co-AM-co-AMPS)/MMT superabsorbent hydrogel. Carbohydr Polym 84:76–82
37. Bulut Y, Akcay G, Elma D, Serhatli E (2009) Synthesis of clay-based superabsorbent composite and its sorption capability. J Hazard Mater 171:717–723
38. Hua S, Wang A (2009) Synthesis, characterization and swelling behaviors of sodium alginate-*g*-poly(acrylic acid)/sodium humate superabsorbent. Carbohyd Polym 75:79–84
39. Zhang YP, Lee SH, Reddy KR, Lee KP (2007) Synthesis and characterization of core-shell SiO_2 nanoparticles/poly(3-aminophenylboronic acid) composites. J Appl Polym Sci 104(4):2743–2750
40. Reddy KR, Raghu AV, Jeong HM (2008) Synthesis and characterization of novel poly urethanes based on 4,4′-{1,4-phenylenebis[methylylidenenitrilo]} diphenol. Polym Bull 60(5):609–616
41. Wang WB, Wang AQ (2010) Nanocomposite of carboxymethyl cellulose and attapulgite as a novel pH-sensitive superabsorbent : synthesis, characterization and properties. Carbohyd Polym 82:83–91
42. Kabiri K, Lashani S, Zouhiriaan-Mehr MJ, Kheirabadi M (2011) Superalcohol-absorbent gels of sulfonic acid-contained poly(acrylic acid). J Polym Res 18:449–458

43. Reddy KR, Lee KP, Gopalan AI (2008) Self-assembly approach for the synthesis of electro-magnetic functionalized FeO/polyaniline nanocomposites: effect of dopant on the properties. Colloid Surf A Physicochem Eng Asp 320(1–3):49–56
44. Işiklan N, Küçükbalcı G (2012) Microwave-induced synthesis of alginate-graft-poly(*N*-isopropylacrylamide) and drug release properties of dual pH- and temperature-responsive beads. E J Pharmacol Biopharm 82:316–331
45. Ganji F, Vasheghani-Farahani S, Vasheghani-Farahani E (2010) Theoretical description of hydrogel swelling: a review. Iran Polym J 19(5):375–398
46. Su JC, Liu SQ, Joshi SC, Lam YC (2008) Effect of SDS on the gelation of hydroxypropylmethylcellulose hydrogels. J Therm Anal Calorim 93:495–501
47. Schott H (1992) Swelling kinetics of polymers. J Macromol Sci B 31:1–9
48. Lanthong P, Kiatkamjornwong S (2006) Graft copolymerization, characterization, and degradation of cassava starch-*g*-acrylamide/itaconic acid superabsorbents. Carbodyd Polym 66:229–245
49. Gils PS, Ray D, Mohanta GP, Manavalan R, Sahoo PK (2009) Designing of new acrylic based macroporous superabsorbent polymer hydrogel and its suitability for drug delivery. Int J Pharm Pharm Sci 1:43–54
50. Hosseinzadeh H, Sadeghzadeh M, Badazadeh M (2011) Preparation and properties of carrageenan—g-poly(acrylic acid)/bentonite superabsorbent composite. J Boimater Nanobiotechol 2:311–317
51. Bulut Y, Gözübenli N, Aydin H (2007) Equilibrium and kinetics studies for adsorption of direct blue 71 from aqueous solution by wheat shells. J Hazard Mater 144:300–306